Thermodynamic stability and optical properties of C-doping-induced defects in hexagonal boron nitride as potential single-photon emitters

Marisol Alcántara Ortigoza[1] and Sergey Stolbov[2,*]

[1]*Physics Department, Tuskegee University, Tuskegee Institute, Alabama 36088, USA*

[2]*Physics Department, University of Central Florida, Orlando, Florida 32816, USA*

(Received 16 December 2021; revised 19 March 2022; accepted 7 April 2022; published 19 April 2022)

Quantum information technologies have triggered enormous interest in single-photon emitters (SPEs), such as local defects in wide-band-gap semiconductors. Recently, visible single-photon emission was observed in carbon-doped hexagonal boron nitride (h-BN), yet the structure giving rise to the emission has not been unambiguously identified. Further progress in the rational design of SPEs requires a deep insight into all the ground-state properties, the electronic structure of the defects in question, and their relationship with the optical properties. To this end, we apply state-of-the-art computational methods to evaluate the stability and optical properties of defects that can be responsible for the above-mentioned experimental findings. For our analysis, we select seven possible C-based defects: (i) C substitutes B (C_B), (ii) C substitutes N (C_N), (iii) C substitutes N and nearest B and N are interchanged (C_NN_B), (iv) C substitutes N and there is a nearby B vacancy (V_BC_N), and (v) three different configurations of V_NC_B (C substitutes B and a nearby N vacancy). We perform calculations of the electronic structure using the linear response approach (*GW* method), followed by finding the solution to the Bethe-Salpeter equation to obtain the excitation spectra of dynamically stable defects. Our density-functional-theory-based calculations of the optimized geometries and their Γ-point phonon frequencies reveal that V_BC_N is dynamically unstable and undergoes a transformation to one corrugated V_NC_B structure. Likewise, the flat V_NC_B (with C_{2v} symmetry) lies on a very shallow and anharmonic minimum that would also relax toward the corrugated V_NC_B structure. Clearly, our results demonstrate how important is to attest to the dynamical stability of any proposed structure. Upon comparing our results of the considered defects with the reported experimental SPE spectra, we show that only the C_N defect has an excitation spectrum fitting the conditions for the observed single-photon emission. Importantly, this defect is found to be the most thermodynamically stable among those under consideration.

DOI: 10.1103/PhysRevB.105.165306

I. INTRODUCTION

High expectations for successful developments in quantum information technologies have triggered enormous interest in single-photon emitters (SPEs) [1]. Of particular interest for their spin and optoelectronic properties [1] are SPEs that are single defects in wide-band-gap semiconductors, such as diamond [2], silicon carbide [3], and hexagonal boron nitride (h-BN) [4–7]. Two-dimensional materials, such as h-BN, have additional advantages because creation of defects in them can be well controlled and they can have other potential applications [1]. Pristine h-BN has a layered hexagonal structure, similar to that of graphene. Like graphene, it can be exfoliated to a single monolayer [5,6]. Yet, in contrast to graphene, it is a wide-band-gap semiconductor: Its band-gap width is ∼6 eV [8,9]. Although this band-gap width corresponds to UV emission, point defects in h-BN may create localized electronic states within the gap, which can become a source of single-photon emission (SPE) in the visible light range. To test this hypothesis, the authors of Ref. [4] performed optical measurements with a laser of 532 nm applied to h-BN samples and detected highly localized photoluminescence emission at around a 623-nm wavelength. Assuming that vacancies and substitutional impurities in h-BN are the source of the corresponding excitations, the authors performed ground-state density-functional-theory (DFT)-based estimates of the transition energies, and concluded that the N vacancy with simultaneous replacement of a B atom with N (V_NN_B) works as the SPE in the h-BN. However, as the authors acknowledged, the generalized gradient approximation for the exchange and correlation functional, which they used in their DFT calculations, fails to predict the band gap because it is not meant to determine the energy of excited states.

In another attempt to reveal the structure giving rise to the observed single-photon emission in h-BN, the authors of Ref. [7] made use of the fact that not only vacancies, but also substitutional impurities may serve as SPEs. Following this idea, the authors of Ref. [7] performed a comprehensive experimental study of the effect of incorporating C, O, and Si into h-BN, and found that only C defects induce the single-photon emission from the system. Various doping technics—such as metal-organic vapor-phase epitaxy, molecular beam epitaxy, and direct ion implantation—were used to dope h-BN with C, and with most techniques the emission was achieved. More specifically, excitation with a 532-nm

*Corresponding author: sergey.stolbov@ucf.edu

(2.33 eV) laser source resulted in an intense emission at 585 nm (the 2.12-eV peak)—associated with the zero-phonon-line—and at 635 nm (the 1.95-eV peak)—interpreted as the phonon sideband peak. To identify the structural configuration generating the observed single-photon emission, the authors performed a computational evaluation of the optical properties of a number of possible defect geometries. Most calculations were performed within the time-dependent density-functional-theory (TDDFT) method to give a better treatment of the excited states than simply ground-state DFT. Various versions of the hybrid potential approximation for the exchange-correlation functional, such as HSE06, HSE06/D3, and CAM-B3LYP, were used in attempt to find the defect that gives rise to the transition matching the experiment. Some of them included the long-range correction. The size of the system under consideration was also varied. Ultimately, the authors picked the negatively charged defect in which C substitutes N and a vacancy is in the neighboring B site ($V_BC_N^-$) as the most fitting defect to the observed SPE. However, comparison of their calculations with the experiment is not conclusive because of significant differences in the energy of the absorption peaks. From another standpoint, other computational results [10,11] have indicated that the V_NC_B defect (vacancy at a N site and C substituting the neighboring B site) with C_{2v} symmetry is the source of emission at an energy of $\sim$2 eV. Unfortunately, the computations also suffer from the inability of ground-state DFT to predict the band structure of excited states. Moreover, the actual geometry of the structure giving rise to the single-photon emission is not altogether clear because, as we shall see later, there are two possible structures that can be considered V_NC_B. In fact, one of them—the one preserving the C_{2v} symmetry—is spin polarized and is the least energetically and thermodynamically stable.

The above-discussed experimental works show that engineering SPEs is achievable. However, a significant progress in the rational design of SPEs is impossible without a deep understanding of all the ground-state properties, the electronic structure of the defects in question, and their relationship with the optical properties, which entirely depends on a reliable characterization of the band structure of the excited states. A substantial contribution to the latter goal can be made by applying state-of-the-art computational methods for the evaluation of the properties of interest, such as the treatment of excited states via the *GW* approximation. Such works already exist. For example, the authors of Ref. [12] have recently applied the *GW* and Bethe-Salpeter equation (BSE) methods to calculate the optical properties of Ti- and Mo-induced defects in h-BN. Another recent study reports on the optical properties of vacancies and C-induced defects in h-BN by applying the GW-BSE methods as well [13]. Importantly, the *GW*-BSE-based study in Ref. [13] shows that the negatively charged $V_BC_N^-$ system and the neutral V_BC_N have a quite different absorption spectrum from that predicted in Ref. [7], which is based on the TDDFT method. On the one hand, the *GW*-BSE formalism applied in Ref. [13] clearly shows that $V_BC_N^-$ cannot be the defect responsible for the single-photon emission because *there are no absorption peaks in the range of absorption/emission*. The *GW*-BSE formalism applied in Ref. [13] shows that the neutral V_BC_N defect displays absorption peaks that pose it as the possible source of the single-photon emission. However, they did not address the dynamical stability of the systems under consideration, which is of critical importance—as we shall see.

In this work we perform spin-polarized DFT calculations of the formation energy and Γ-point vibrational spectra, as well as *GW*-BSE calculations of the electronic structure and optical properties of C-doping related defects in h-BN. The optical properties of a defect are of interest only if the defect is dynamically stable, because otherwise it cannot even exist. We thus start with a computational evaluation of the defect stability. We select seven defects: C_B (C substitutes B), C_N (C substitutes N), C_NN_B (C substitutes N and nearest N is interchanged with B), V_BC_N, and three different configurations of V_NC_B: two configurations in which there is a N-vacancy plus C substitutes B: V_NC_B (C_{2v}, because of its symmetry) and V_NC_B (corrugated, with the lower C_1 symmetry), and one asymmetric configuration, V_NC_B [asymmetric, because C and one neighboring N are swapped with respect to $V_NC_B(C_{2v})$]. Using DFT-based methods, we calculate the formation energy of the defects and their dynamical stability. Next, for the defects we find to be stable, we perform a *GW* calculation of the density of states of independent quasiparticles within the linear response approximation [14]. Finally, to evaluate the optical excitations in the dynamically stable systems, we obtain the imaginary part of the frequency-dependent dielectric function and the oscillator strengths by applying the BSE method [15], which takes into account exitonic effects. The final identification of the C-induced defect in h-BN that acts as the SPE obtained in the experiment [7] is based on the notion that it must have high-probability excitations in the energy region between 2.33 eV, the laser excitation energy used in the experiment, and 2.12 eV, which the intense emission peak energy detected in Ref. [7].

II. COMPUTATIONAL DETAILS

All calculations in this work were performed using the Vienna Ab-initio Simulation Package VASP5.4 [16]. Pristine h-BN was modeled by one monolayer (ML) of (1×1) in-plane periodicity and a (4×4) in-plane periodicity. Thus, to sample the Brillouin zone of pristine h-BN, we use a $(16 \times 16 \times 1)$ k-point mesh and $(4 \times 4 \times 1)$ k-point mesh, respectively. The defected h-BN systems were modeled by one h-BN layer in a hexagonal supercell of 4×4 in-plane periodicity and a 16.4-Å long c-translation vector. The 1×1 and 4×4 supercells include 2 and 32 atoms, respectively. A cutoff energy of 400 eV was used for the plane-wave expansion of wave functions and a $(4 \times 4 \times 1)$ k-point mesh was used to sample the Brillouin zone. These values provided convergent results for the characteristics of interest. All calculations allowed for spin-polarization of the systems.

The formation energy of the defects and phonon spectrum of the systems were calculated within DFT with projector-augmented-wave potentials [17] and the Perdew-Burke-Ernzerhof (PBE) parametrization for the exchange and correlation functional [18]. During structural relaxation, the atomic positions were iteratively optimized until the forces acting on each atom in each direction did not exceed 0.0015 eV/Å.

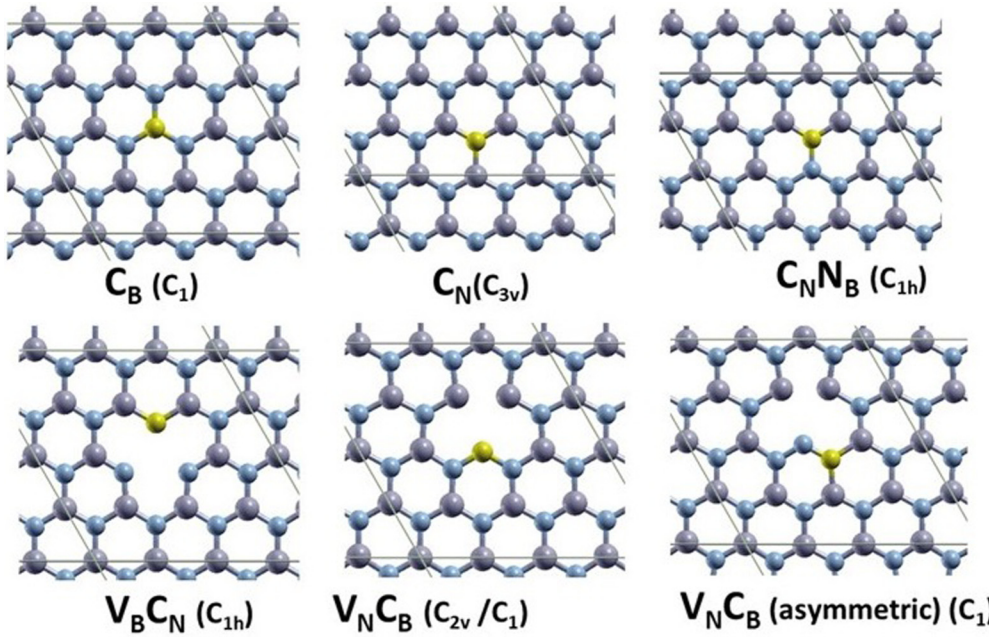

FIG. 1. The seven defects considered in this work. Grey, blue, and yellow balls represent B, N, and C atoms, respectively. The defects are plotted in the monolayer plane with atom positions after the relaxation. The point symmetry of the defects is provided in parentheses. V_BC_N (C_{2v}) and V_BC_N(corrugated) are represented in the same figure because the geometric differences between the two are not recognizable to the naked eye from the top view.

The vibrational frequencies and displacement patterns of the various systems under investigation were calculated at the Γ point using the finite difference method, as implemented in VASP5.4. To obtain the force constant matrix, the forces on the atoms were obtained by total energy calculations upon displacing each atom along all six Cartesian directions. The magnitude of displacement along each direction was 0.015 Å. Nevertheless, dynamical stability was further confirmed for displacements of 0.05 Å and more when needed.

The electronic structure, via the independent quasiparticle (IQP) densities of states (DOSs), was calculated within the random phase approximation (RPA) by performing the first iteration of Hedin's equations within the *GW* approximation for the self-energy, known as the G_0W_0 approximation [19]. The linear response function was calculated for 50 frequencies using 192 bands with a cutoff energy of 85 eV. The quasiparticle energies were calculated for 128 bands. To obtain the frequency dependent dielectric function and the optical oscillator strengths, we used the BSE method, which takes into account the electron-hole interaction (excitonic effects). For all defected systems under consideration, 40 occupied and 24 unoccupied *GW* bands were included in the BSE treatment. The included frequencies ranged between 0 and 20 eV. The BSE couples the ground and excited states with the same spin and k vector. It thus results in the dipole spin-preserved radiative transitions in the reciprocal-space representation.

III. FORMATION ENERGIES OF C-DOPING DEFECTS IN h-BN

To reveal the energetically preferred C-based defects in h-BN, the formation energies E_{form} of the C_B, C_N, C_NN_B, V_BC_N, $V_NC_B(C_{2v})$, V_NC_B(corrugated), and V_NC_B(asymmetric) defects were calculated. The corresponding structures are illustrated in Fig. 1. This selection includes the most trivial C_B and C_N defects, C_NN_B, which is in fact C_B with interchanged C and N atoms, V_BC_N (which has been studied in Refs. [7] and [13]), and two configurations for the V_NC_B defects: V_NC_B (C_{2v}), a structure in which the vacancy and the substitutional carbon atoms have C_{2v} symmetry (considered in Ref. [10] as the SPE in C-doped h-BN), V_NC_B(corrugated), a highly corrugated structure that has much lower symmetry than V_NC_B (C_{2v}), and V_NC_B(asymmetric), also a highly corrugated structure that is asymmetric by construction.

The formation energy (E_{form}) of the considered C-based defects in h-BN is determined as follows:

$$
\begin{aligned}
&E_{\text{form}}(\mathrm{C_B}) \\
&\quad = E_{\text{tot}}(\mathrm{C_B}) + \mu(\mathrm{B}) - E_{\text{tot}}(\mathrm{BN}) - \mu(\mathrm{C}), \\
&E_{\text{form}}(\mathrm{C_N}) \\
&\quad = E_{\text{tot}}(\mathrm{C_N}) + \mu(\mathrm{N}) - E_{\text{tot}}(\mathrm{BN}) - \mu(\mathrm{C}), \\
&E_{\text{form}}(\mathrm{C_NN_B}) \\
&\quad = E_{\text{tot}}(\mathrm{C_NN_B}) + \mu(\mathrm{B}) - E_{\text{tot}}(\mathrm{BN}) - \mu(\mathrm{C}), \\
&E_{\text{form}}(V_{\mathrm{B}}\mathrm{C_N}) \\
&\quad = E_{\text{tot}}(V_{\mathrm{B}}\mathrm{C_N}) + \mu(\mathrm{B}) + \mu(\mathrm{N}) - E_{\text{tot}}(\mathrm{BN}) - \mu(\mathrm{C}), \\
&E_{\text{form}}(V_{\mathrm{N}}\mathrm{C_B}C_{2v}/\text{corrugated}) \\
&\quad = E_{\text{tot}}(V_{\mathrm{N}}\mathrm{C_B}C_{2v}/\text{corrugated}) + \mu(\mathrm{B}) + \mu(\mathrm{N}) \\
&\qquad - E_{\text{tot}}(\mathrm{BN}) - \mu(\mathrm{C}), \\
&E_{\text{form}}(V_{\mathrm{N}}\mathrm{C_B}\text{asymmetric}) \\
&\quad = E_{\text{tot}}(V_{\mathrm{N}}\mathrm{C_B}\text{asymmetric}) + \mu(\mathrm{B}) + \mu(\mathrm{N}) \\
&\qquad - E_{\text{tot}}(\mathrm{BN}) - \mu(\mathrm{C}).
\end{aligned}
$$

TABLE I. Formation energy of the C-doping-induced defects in h-BN and corresponding binding energy.

	E formation (eV)			
	N rich	N poor	μ (atom)	Binding energy of C
C_B	1.945	4.553	2.417	-13.20
$C_N N_B$	4.964	7.572	5.436	-10.547
C_N	3.776	0.167	0.823	-11.342
$V_B C_N$	9.234	9.234	14.725	-7.277
$V_N C_B(C_{2v})$	7.950	7.950	13.441	-8.460
$V_N C_B$(corrugated)	7.374	7.374	12.865	-9.137
$V_N C_B$(asymmetric)	7.979	7.979	13.470	-8.532

Here E_{tot}(BN) is the DFT total energy calculated for pristine h-BN. E_{tot}(defect) is the DFT total energy per supercell calculated of defected h-BN, where defect $= C_B$, C_N, $C_N N_B$, $V_B C_N$, $V_N C_B(C_{2v})$, $V_N C_B$(corrugated), and $V_N C_B$ (asymmetric). $\mu(X)$ is the chemical potential of X, where $X =$ B, N, and C atoms. The chemical potential $\mu(X)$ depends on the conditions around the defect formation: the nitrogen-rich condition, the nitrogen-poor condition, and the condition in which the space around the system is empty (one atom just replaces another). For the nitrogen-rich condition, $\mu(B) = \mu(BN) - 0.5E_{tot}(N_2)$ and $\mu(N) = 0.5E_{tot}(N_2)$. For the N-poor condition, we use the cohesive energy of bulk B plus the total energy of a free B atom as $\mu(B)$, and $\mu(N) = \mu(BN)$-$\mu(B)$. Here $\mu(BN)$ is the chemical potential of BN, determined as the DFT total energy of the 1×1 primitive (two-atom) unit cell of pristine h-BN, and $E_{tot}(N_2)$ is the DFT total energy of a free nitrogen molecule. For μ(C), we use the cohesive energy of graphene plus the total energy for a free C atom. For the condition in which the space around the system is empty, $\mu(X)$ is equal to the total energy of the corresponding X atom. The formation energies calculated for the defects using the above conditions are listed in Table I. We also provide the binding energy of the C atom [E_B(C)] in the defected structures.

We considered two local energy minima for the $V_N C_B$ defect $-V_N C_B(C_{2v})$ and $V_N C_B$(corrugated)—though their differences in geometric structure are not recognizable from the top view to the naked eye (see Fig. 1).

As seen from the table, the C_N and C_B defects have the lowest formation energy, while the C doping accompanied by a neighboring vacancy leads to much higher E_{form}. All considered defects have a positive E_{form}, which means that the formation of each defect is an endothermic process and energetically unfavorable. But that does not mean that these defects cannot exist. It is impossible, for example, to induce C desorption from $V_N C_B$ by standard annealing furnaces ($\sim$2000 K) because the binding energy of C in $V_N C_B(C_{2v})$ is as high as 8.46 eV. Filling the N vacancy in this defect by reaction with an N_2 molecule is thermodynamically favorable, however, it can be achieved only by breaking the equally strong chemical bond of N_2 (9.9 eV). Therefore, even though the formation energies of these defects are positive, the microkinetics of the systems is what determines whether they will survive for microseconds or years (locally stable for application purposes). However, there is an even more important factor in determining the stability of a defect, which is dynamical stability (see Sec. IV).

It calls our attention that, to the naked eye and from the top view, the $V_N C_B$(corrugated) structure looks identical to the $V_N C_B(C_{2v})$ structure, yet the C atom is significantly out of the ML plane and the structure in general is corrugated. Moreover, unlike the $V_N C_B(C_{2v})$ structure, the $V_N C_B$(corrugated) structure is nonmagnetic. The total energy of $V_N C_B$(corrugated) is 0.576 eV lower than that of the $V_N C_B(C_{2v})$ structure. We propose the following explanation for the above effects. Since the C atom has in-plane position in $V_N C_B(C_{2v})$, its p_z states are orthogonal to the in-plane sp^2 states and therefore there is no hybridization between these states. Then, the hybridization between p_z states of C and neigboring N atoms is weak due to π symmetry. These factors make favorable spin polarizaition associated with Cp_z states. The displacement of C from the plane lifts the orthogonality and thus involves the Cp_z states in hybridization with the sp^2 states, which leads to a decrease in the total energy and makes spin polarization unfavorable. In addition, this hybridization breaks the sp^2 symmetry around the defect resulting in the corrugation.

IV. DYNAMICAL STABILITY OF C DEFECTS IN h-BN

Calculation of the vibrational frequencies of a proposed structure is a prime tool to verify its plausibility. In the case of single defects in wide-band-gap semiconductors aimed at serving as SPEs, only dynamically *stable* structures can be expected to have a lifetime suitable for applications or at least for optical characterization after synthesis. A structure is dynamically stable if its force constant matrix yields real-valued eigenfrequencies, which means that the corresponding eigenmodes will make the atoms oscillate around their equilibrium positions. In contrast, a structure is dynamically *unstable* if its force constant matrix yields one or more imaginary eigenfrequencies, which means that the corresponding eigenmode(s) would make the atoms displace in such a way that they will not come back to the original equilibrium positions but move barrierless to another equilibrium configuration of lower energy, even at 0 K.

We find that C_B, C_N, $C_N N_B$, $V_N C_B(C_{2v})$, $V_N C_B$(corrugated), and $V_N C_B$(asymmetric) are dynamically stable. In other words, only the $V_B C_N$ structure is dynamically unstable. This is important for several reasons: the negatively charged $V_B C_N^-$ structure has been proposed in Ref. [7] to be the SPE emitting single photons of 585 nm. Reference [13] has shown through state-of-the-art GW-BSE calculations that $V_B C_N^-$ does not have the optical properties of the observed SPE. Still, the optical properties reported in Ref. [13] hint that neutral $V_B C_N$ might be the SPE. Yet, here we find that $V_B C_N$ should not be even considered because it is *dynamically unstable*. That is, one of its vibrational modes, which largely involves an in-plane displacement of the substitutional C atom, has an imaginary frequency of 23.94 meV. This result clearly indicates that the $V_B C_N$ structure cannot exist long enough to sustain the experimental handling and give rise to the reported observations. We forbore verifying whether or not $V_B C_N^-$ is dynamically stable because, interestingly, the authors of Ref. [7] reported that the charged $V_B C_N^-$ structure renders some "small imaginary frequencies," which they

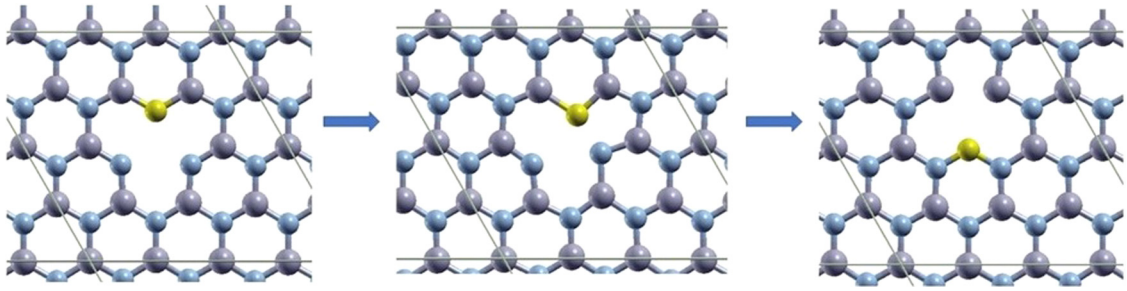

FIG. 2. Transformation of V_BC_N into V_NC_B(corrugated) caused by the dynamical instability of V_BC_N and that of the two subsequent two intermediate configurations. (a) V_BC_N, (b) second intermediate configuration, (c) V_NC_B(corrugated). Grey, blue, and yellow balls represent B, N, and C atoms, respectively.

ignored. However, the actual value was not reported. In our calculations the imaginary frequency of the neutral V_BC_N is 23.94 meV, which is not small by any means. It is important to note that, in principle, a stable structure should not render *any* imaginary mode regardless of whether it is small or large. There are, however, three "translational" acoustic modes for any extended structure that must have exactly zero frequency [20,21]. These modes are those in which none of the atomic bonds is stretched, instead the whole system translates in one of the three Cartesian directions. Nevertheless, because of small computational errors, the frequencies of these translational modes may be nonzero positive or imaginary, but their magnitude does not exceed 1 or 2 meV [21,22]. In our calculations, all stable structures have exactly three translational modes in that range. Yet, as mentioned before, V_BC_N structure has an imaginary frequency of 23.94 meV that mostly involves the C atom, in addition to the three translational modes.

Thus, the question arises as to whether the unstable mode of V_BC_N would drive it toward a local minimum configuration that would essentially preserve the V_BC_N structure [see Fig. 2(a)] and, more importantly, the optical properties found in Ref. [13]. We searched such a nearest local minimum configuration by first using the displacement pattern of the unstable vibrational mode of the V_BC_N structure. That is, the atomic positions of the V_BC_N structure [7,13] were perturbed following the displacement pattern of the unstable mode and then the structure was rerelaxed. Finding the nearest local minimum configuration in this manner was not a one-step procedure, as illustrated in Fig. 2. Namely, the potential energy surface has apparently several saddle points and shallow minima around this structure. For example, after perturbing the structure as hinted by the displacement pattern of the unstable mode of the V_BC_N structure, the atoms relaxed toward another saddle-point configuration that is 0.188 eV higher in energy than the V_BC_N structure. This new structure turned out to be the first intermediate configuration toward the final local minimum configuration. In this first intermediate structure, carbon gets slightly closer to one of the B atoms than to the other and becomes non-spin-polarized. Nevertheless, this first intermediate structure is also dynamically unstable and thus a saddle point. We thus used again the displacement pattern of this unstable mode of the first intermediate structure to change the atomic positions and rerelaxed the structure. Although this unstable mode led us again to a saddle-point structure in which C gets even closer to one B atom, in this new configuration C also starts binding to a N atom [see Fig. 2(b)] and the energy drops by 0.170 eV below the total energy of the V_BC_N structure. This second new structure, which is also nonmagnetic, turned out to be the second intermediate configuration toward the final local minimum configuration. Since this second intermediate configuration is also dynamically unstable, we yet again used its unstable mode (once more, mostly involving the C atom) to lead us to a local minimum configuration. Upon perturbing the atomic positions of the second intermediate structure—as prescribed by its unstable mode—the system relaxed toward the V_NC_B(corrugated) structure [see Fig. 2(c)], in which C strongly binds to two N atoms and the energy drops significantly, 1.860 eV below the total energy of the V_BC_N structure. It is worth mentioning that the authors of Refs. [7] and [23] also found several local minima around V_BC_N.

The above calculations, following the displacement pattern of the unstable modes (all of them mostly involving the C atom), show that even if a C atom initially binds to the two dangling B atoms of the V_BV_N divacancy defect, the natural vibrations will quickly destabilize the resulting V_BC_N structure and drive the C atom to a series of transitions until it binds to the two dangling N atoms, forming the V_NC_B(corrugated) structure. In other words, regardless of the optical properties obtained in Refs. [7] and [13], the V_BC_N structure simply cannot be the C-based single-photon emitter (SPEs) reported in Ref. [7] because it is dynamically unstable.

We now turn to the case of $V_NC_B(C_{2v})$. This defect is also important because it has been proposed that it is the defect that gives rise to the single-photon emission [10]. The first feature that calls our attention regarding its stability is that the rigid translational mode in the off-plane direction perpendicular to the monolayer plane has an imaginary frequency larger than few meV, i.e., ∼12 meV for displacements of 0.015 Å, and it is not a perfectly rigid mode since the C atom and the two neighboring low-coordinated B atoms have a larger amplitude than the rest. This is common when the local minimum is very shallow or intrinsically anharmonic with respect to the perturbation of some bond(s). In such cases the total energy—which is used to get the force constant matrix—hardly changes upon the perturbation of some bond(s). Indeed, the increase in total energy when C (and neighboring B atoms) is displaced in the vertical direction by 0.015 Å is only 0.7 meV (definitely smaller than the method error). One would expect that a larger displacement of the atoms to get the force constant matrix would resolve the issue of the relatively large imaginary frequency, and it does to some degree. If the displacement

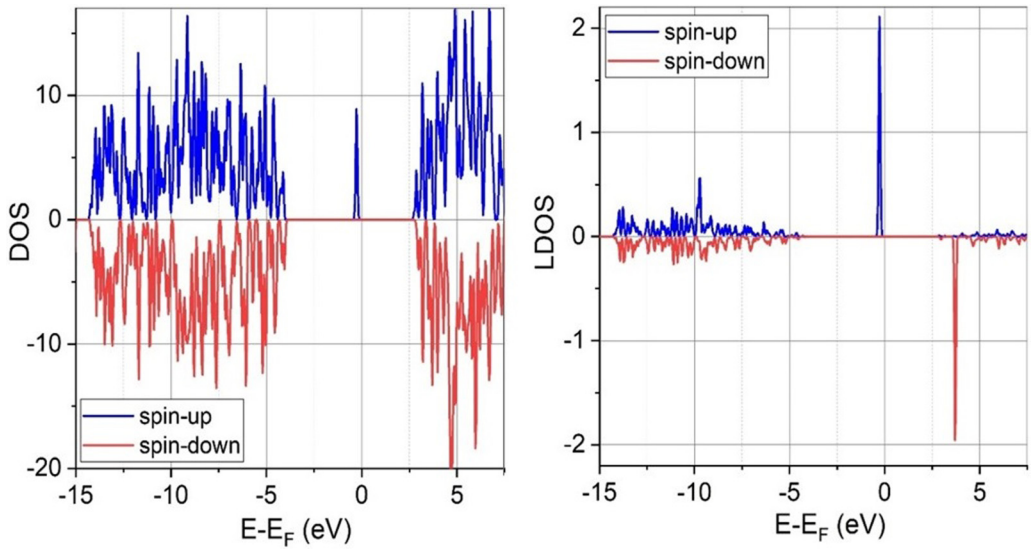

FIG. 3. Electronic structure of the C_B-defected h-BN calculated within the *GW* approximation. Left panel: total density of IQP states. Right panel: density of the carbon *p* states.

increases to 0.05 Å, the rigid-translation mode renders an imaginary frequency of 9 meV. That imaginary frequency is still too large, but not surprisingly so, since the increase in total energy upon displacing C in the vertical direction by 0.05 Å is in this case only 7 meV (yet the increase in total energy for the same displacement for low-coordinated neighboring B atoms is much larger in this case). If the displacement of C to determine the force constant matrix increases to 0.07 Å, the rigid-translation mode renders an imaginary frequency of 5.5 meV. That imaginary frequency is still too large and the change in energy clearly indicates that anharmonicity sets in.

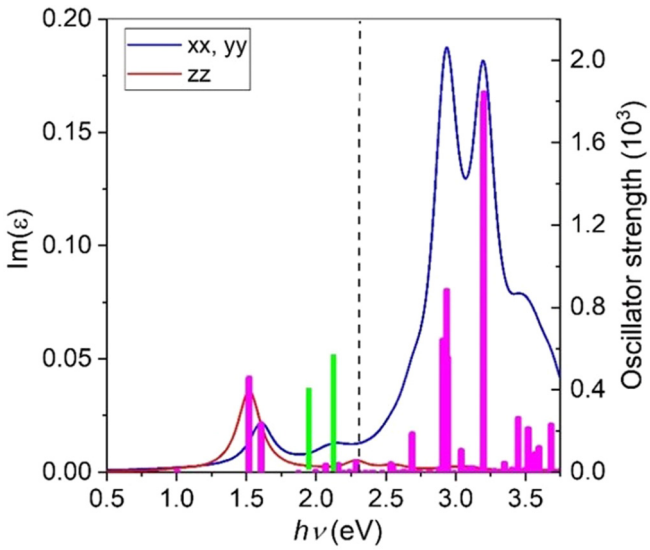

FIG. 4. The imaginary part of the frequency-dependent dielectric function (continuous lines) for *xx*, *yy* (blue), and *zz* polarization (red), and the oscillator strength of the dipole optical transitions (pink vertical lines) calculated for the C_B defected h-BN. The green lines mark the energetic positions of the emission detected in Ref. [7]. The dashed black line marks the laser excitation energy 2.33 eV used in Ref. [7].

Finally, for displacements of 0.1 Å, the imaginary frequency became ∼1 meV. However, we noticed that for displacements of 0.1 Å other low-lying modes involving C are fully driven to the anharmonic regime. Therefore, we turned to check the stability of $V_NC_B(C_{2v})$ in terms of the energy barrier toward another minimum. To that end, we evaluated the response of $V_NC_B(C_{2v})$ to similar perturbations as those used to get the force constant. We displaced the C atom perpendicular to the monolayer plane by several displacements Δz. We found that for $\Delta z = 0.085$ Å, the system starts to have a magnetic instabilty (as the C moves further away from its neighbors the magnetization decreases), which is accompanied by an instability of the ground state electronic structure and, consequently, of the total energy and forces (i.e., these quantities either do not converge or their values depend on the initial wave functions). Nevertheless, *regardless of these instabilities*, we found that, if Δz is smaller or equal to 0.095 Å, the structure somehow relaxes back to $V_NC_B(C_{2v})$. However, for larger Δz and *despite the instabilities*, the structure is transformed to the lower energy structure: V_NC_B(corrugated). Interestingly, if $\Delta z = 0.095$ Å, before structural relaxation, the system still seems to be magnetic and the total energy is, as expected, higher than that of $V_NC_B(C_{2v})$. However, if $\Delta z = 0.1$ Å and *despite the instabilities*, even before structural relaxation, the magnetization is already zero. Then, upon structural relaxation, and despite the initial instabilities, the structure and total energy consistently becomes that of V_NC_B(corrugated). We can thus conclude that not only is the $V_NC_B(C_{2v})$ structure a local minimum with total enery higher than that in V_NC_B(corrugated), but it also is a very shallow minimum, making its stability rather weak. In other words, the $V_NC_B(C_{2v})$ struture will transform to V_NC_B(corrugated) once the amplitude of the vibrations of C exceeds 0.1Å. It would require to calculate the mean-squared amplitude as a function of temperature to find out the temperature at which the transtion would take place. However, one can estimate that it would occur around room temperature, as k_BT at room temperature corresponds to 25 meV, which is comparable to

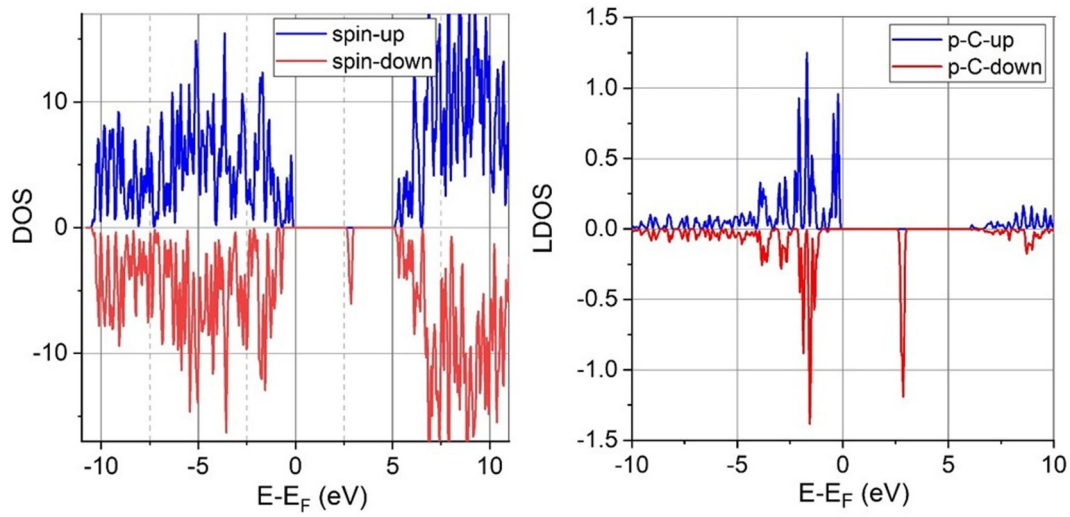

FIG. 5. Electronic structure of the C_N-defected h-BN calculated within the *GW* approximation. Left panel: total density of IQP states. Right panel: density of the carbon *p* states.

the excitation energy of the lowest frequency mode of the system that involves mostly C. But this just brings us back to the original question of whether $V_NC_B(C_{2v})$ is dynamically stable or not. Since the system becomes electronically unstable already for $dz = 0.085$ Å, our phonon calculations for displacements of 0.1 Å are not reliable and thus do not convincingly demonstrate that the imaginary frequency of the off-plane translational mode of $V_NC_B(C_{2v})$ vanishes. Nevertheless, we conclude that the system is dynamically stable at low temperatures because that off-plane translational mode displaces C with respect to the rest of the atoms by only an amount that is not sufficiently large to drive the reconstruction.

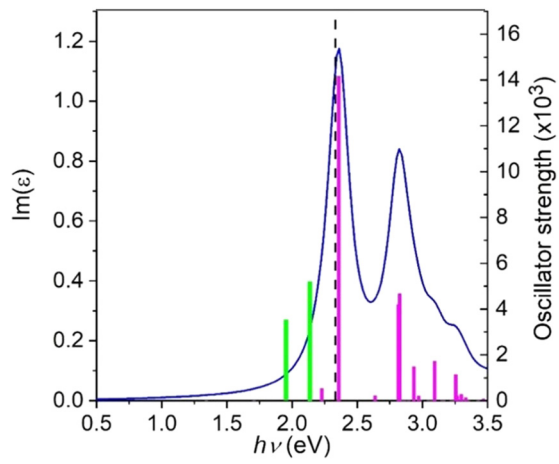

FIG. 6. The imaginary part of the frequency-dependent dielectric function (continuous lines) for *xx*, *yy* (blue), and *zz* polarization (red), and the oscillator strength of the dipole optical transitions (pink vertical lines) calculated for the C_N defected h-BN. The green lines mark the energetic positions of the emission detected in Ref. [7]. The dashed black line marks the laser excitation energy 2.33 eV used in Ref. [7].

V. ELECTRONIC STRUCTURE AND OPTICAL PROPERTIES OF THE C-DOPING INDUCED DEFECTS IN h-BN

To evaluate the electronic structure of the defected h-BN, we calculated the spin-resolved densities of the IQP within the *GW* approximation. In Ref. [7], the emisson at $h\nu = 2.12$ eV was induced by a laser of 2.33 eV. The *necessary* condition for this process to happen is the availability of high probability exitations (i.e., with high oscillator strength) in the system that have an energy E_{exc} $(= h\nu)$ in the range $2.12\,\text{eV} < E_{exc} < 2.33\,\text{eV}$. To check this condition, we calculate (applying the BSE method) and analyze the imaginary part of the frequency-dependent dielectric function and the oscillator strengths for all excitations within this range for the six dynamically stable defects. We of course omit here V_BC_N because it is dynamically unstable. However, in our preliminary calculations for convergence, we verified that the absorption spectrum we obtained for V_BC_N is in excellent agreement with that reported in Ref. [13].

A. C_B defect

The substitution of boron with a C atom in the C_B defect brings an extra valence electron to the system. This leads to the formation of an occupied local peak of DOS in the middle of the band gap and an unoccupied peak inside the conduction band of h-BN (see Fig. 3). As seen from the right panel of Fig. 3, these peaks are formed by *p* states of carbon. The peaks have opposite spin polarization, which results in a magnetization of $1.0\mu_B$ per supercell, though some traces of spin density are found on other (mostly N) sites. We find that, in the optimized structure, the C atom is off plane by 0.16 Å leading to a broken in-plane symmetry. Nevertheless, according to our analysis, the Cp_x and Cp_y states are involved in the sp^2 hybridization, which results in strong bonds with the neighboring N atoms, whereas the Cp_z states make weak π-symmetry bonds, which leaves these states spin polarized.

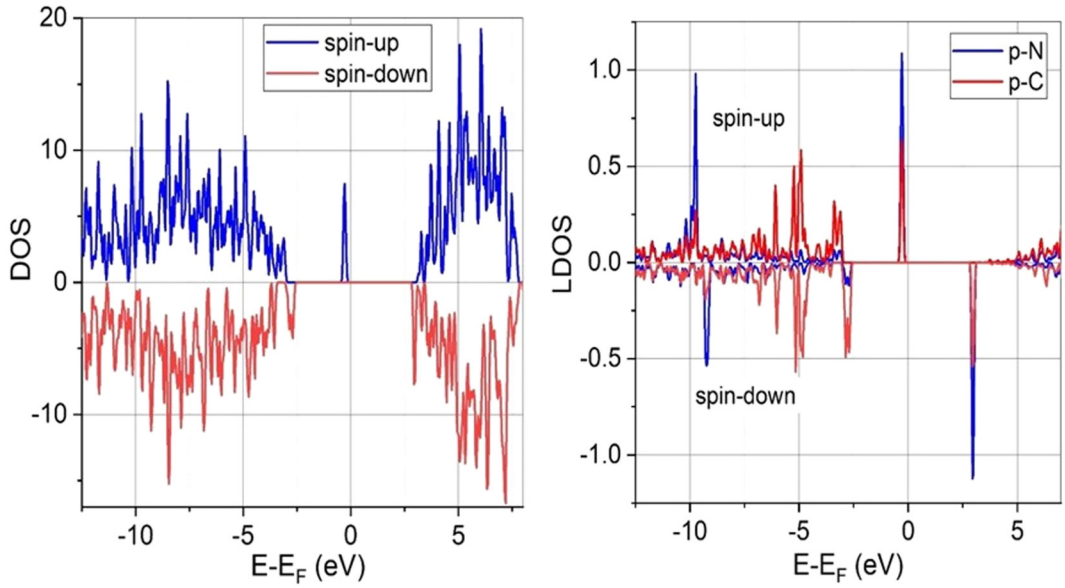

FIG. 7. Electronic structure of the C_NN_B defected h-BN calculated within the *GW* approximation. Left panel: total density of IQP states. Right panel: density of the *p* states of C and the neighboring N atom.

Since we are interested in the optical properties of the defect within the visible spectrum, it is important to note that, in the case of the C_B defect, the excitations leading to such SPE properties may be from a narrow initial state in the local occupied peak in the middle of the band gap to a wide range of final states in the conducting band (CB).

Much more information about optical properties can be obtained from the frequency-dependent dielectric function $\varepsilon(\omega)$ as well as from the oscillator strength of the dipole optical transitions because the oscillator strength characterizes the probability of the transition (see pink bars in Fig. 4). These two characteristics, calculated for C_B defected h-BN within the BSE method, are plotted in Fig. 4. Note that only the range of interest (0.5–3.75 eV) is shown in the figure. As seen from the figure, due to the symmetry of the defect, the *xx* and *yy* polarizations of Im(ε) are degenerated. One can see that there are two minor absorption peaks just above 1.5 eV, some absorption peak of very low oscillator strength values in the region between 2.0 and 2.5 eV, and relatively intense peaks between 2.8 and 3.2 eV. A necessary condition for the emission reported in Ref. [7] is that the intensive absorption peaks lie in the range between the observed emission energy (2.12 eV) and the laser excitation energy (2.33 eV). The excitation structure obtained for C_B does not meet this condition. Therefore, we conclude that the C_B defect in the h-BN is unlikely to be the source of SPE reported in Ref. [7]. Nevertheless, the absorption peaks around 1.5 eV may cause emission in the near-infrared region, which is of high interest to quantum optics.

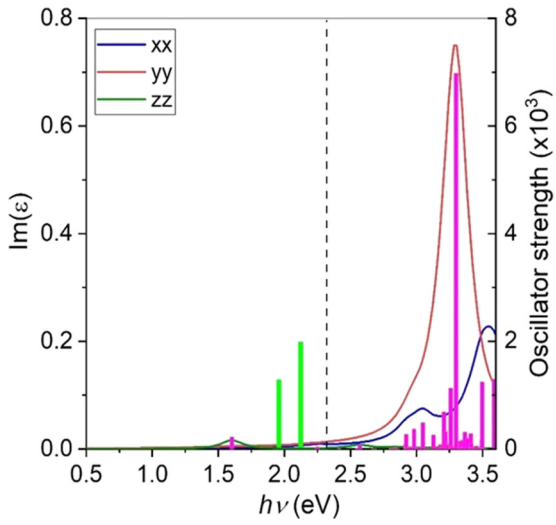

FIG. 8. The imaginary part of the frequency-dependent dielectric function (continuous lines) for *xx* (blue), *yy* (red), and *zz* polarization (green), and the oscillator strength of the dipole optical transitions (pink vertical lines) calculated for the C_NN_B defected h-BN. The green lines mark the energetic positions of the emission detected in Ref. [7]. The dashed black line marks the laser excitation energy 2.33 eV used in Ref. [7].

B. C_N defect

The substitution of N by C in the C_N defect reduces the number of valence electrons in the system by 1. Our computational results show that the creation of the C_N defect leads to the formation of two occupied peaks right next to the top of the valence band (VB)—which effectively narrow the band gap—and a narrow peak of unoccupied states of opposite spin in the middle of the band gap. These three peaks originate from the *p* states of carbon (see Fig. 5). In this defect, C lies in the ML plane. Therefore, according to our analysis, the Cp_x and Cp_y states are involved in the sp^2 hybridization, which results in strong bonds with the neighboring B atoms; while the Cp_z states display only weak π-symmetry bonding and thus remain spin polarized, which is in agreement with results reported in Ref. [24]. The latter results in the magnetization of the supercell by $1.0\mu_B$, and is mostly localized at the C atom,

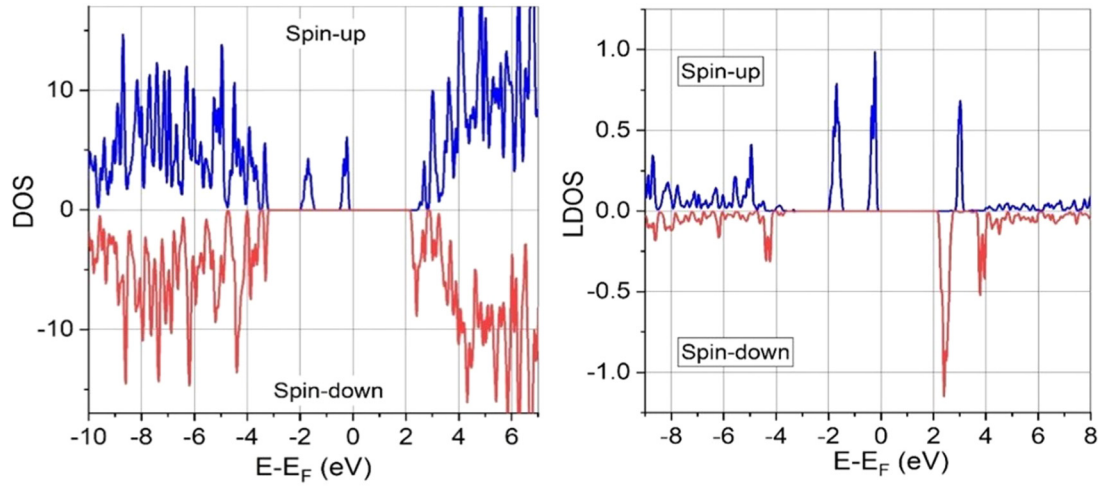

FIG. 9. Electronic structure of the $V_NC_B(C_{2v})$-defected h-BN calculated within the *GW* approximation. Left panel: total density of IQP states. Right panel: density of the carbon *p* states.

though some very minor spin density is distributed over the next-nearest-neighboring N atoms.

As seen from Fig. 5, the excitation of interest can have a wide range of initial states in the VB and a narrow range of final states at the peak in the middle of the band gap.

The imaginary part of the dielectric function and the oscillator strengths calculated for the C_N defect are shown in Fig. 6. According to the calculations, the *zz* component of Im(ε) has a negligible magnitude in the energy range of interest, and the *xx* and *yy* components are degenerated. We find that there is no noticeable absorption for energies below 2 eV, while two sharp and intense peaks appear around the excitation energy range 2.3–2.7 eV. If we focus again on the region of $2.12\,\text{eV} < h\nu < 2.33\,\text{eV}$—searching for an intensive adsorption necessary for the emission reported in Ref. [7]—we find that the C_N defected h-BN results in a very intense oscillator strength peak situated at $h\nu = 2.36\,\text{eV}$. This is only 30 meV above the laser photon energy used in Ref. [7]. Considering the finite width of the excited states, and that the accuracy of the calculations is not perfect, we may conjecture that the excitation associated with this peak can be achieved in the conditions reported in Ref. [7] and thus conclude that the C_N defected h-BN can be responsible for the single-photon emission reported in Ref. [7].

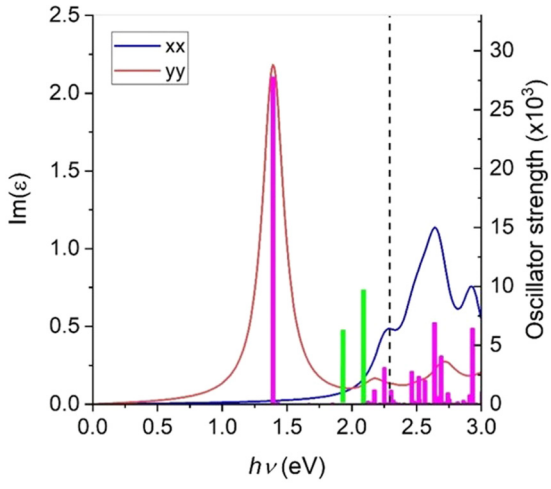

FIG. 10. The imaginary part of the frequency-dependent dielectric function (continuous lines) for *xx*, *yy* (blue), and *zz* polarization (red), and the oscillator strength of the dipole optical transitions (pink vertical lines) calculated for the $V_NC_B(C_{2v})$-defected h-BN. The green lines mark the energetic positions of the emission detected in Ref. [7]. The dashed black line marks the laser excitation energy 2.33 eV used in Ref. [7].

C. C_NN_B defect

The C_NN_B defect forms a flat structure—all atoms are in the ML plane. Formation of this defect leads to the addition of one extra electron to the system. As a result, an occupied local peak of DOS is formed in the middle of the band gap. In addition, one extra peak is formed right above the top of the VB and the other just below the bottom of the CB, leading to the reduction of the band gap. The main contribution to these peaks is made by the *p* states of C and the neighboring N atoms (see Fig. 7). The system is found to be magnetic with a magnetization of $1.0\mu_B$ per supercell. The spin density is mostly localized on C and the neighboring N atoms, with some small contribution from other N atoms. Again, the sp^2 hybridization involves the p_x and p_y states of C and the neighboring N atoms in covalent bonding, while the p_z states of both atoms remain weakly hybridized, and thus available for spin polarization.

The initial states for low energy excitations in the C_NN_B defect can be located only in the narrow DOS peak in the middle of the bad gap, while the final states are situated in the wide CB. The *yy* component of the imaginary part of the dielectric function displays an intense peak at $h\nu \sim 3.5$ eV (see Fig. 8). The *xx* component has some structure in the 3.0–3.5-eV range, while the *zz* component has a negligible intensity in the energy range of interest. The only intense oscillator strength peak is located at $h\nu = 3.3\,\text{eV}$, which is much higher than the energy of the exciting laser radiation (2.33

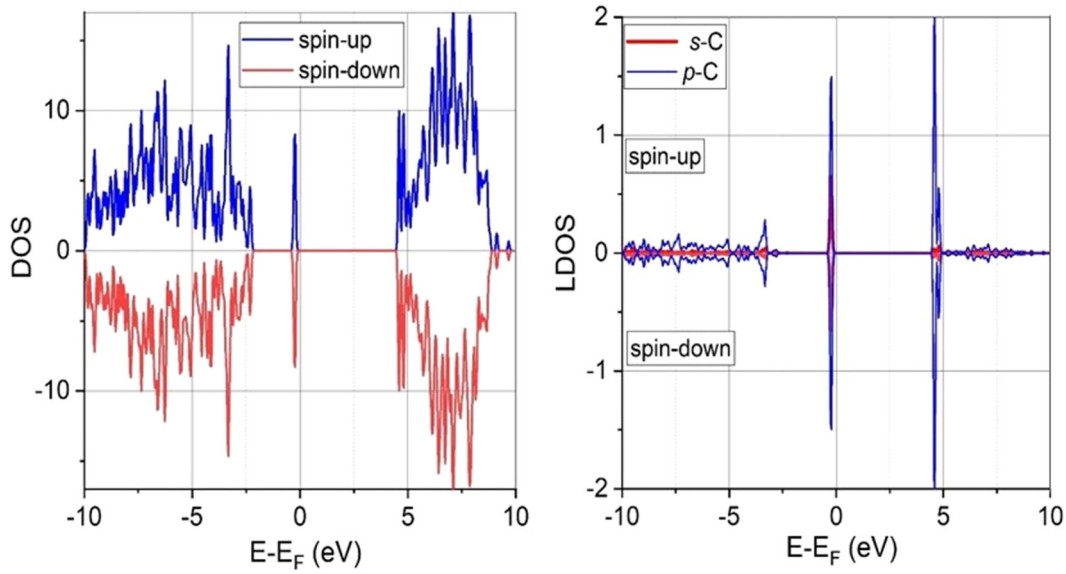

FIG. 11. Electronic structure of the V_NC_B(corrugated) defected h-BN calculated within the *GW* approximation. Left panel: total density of IQP states. Right panel: density of the carbon *s* and *p* states.

eV). Therefore, we conclude that the C_NN_B defect cannot be the source of the single-photon emission detected in Ref. [7].

D. $V_NC_B(C_{2v})$ defect

The $V_NC_B(C_{2v})$ defect forms a flat structure—all atoms are in the ML plane. This defect reduces the number of valence electrons in the system by 2. As described earlier, the C atom is spin polarized in this structure leading to the total magnetization of $2.0\mu_B$. The spin density is almost entirely localized on the C atom. It is associated with two narrow occupied peaks of DOSs formed within the gap (see Fig. 9). The main contribution to these peaks is made by the Cp_Z states. As seen

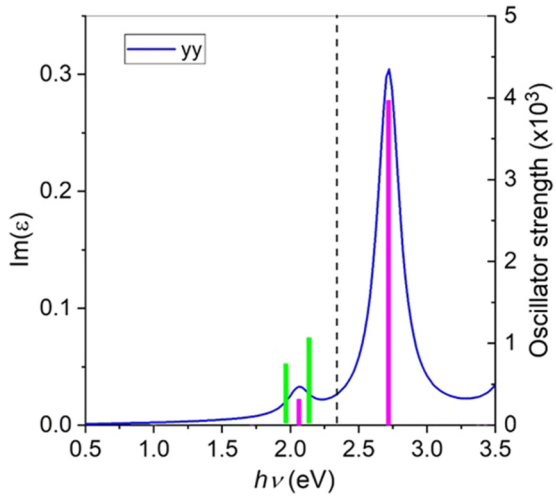

FIG. 12. The *yy* component of the imaginary part of the frequency-dependent dielectric (blue continuous line) and oscillator strength of the dipole transitions (pink vertical lines) calculated for the V_NC_B(corrugated) defected h-BN. The green lines mark the energy of the emission detected in Ref. [7]. The dashed black line marks the laser excitation energy 2.33 eV used in Ref. [7].

from the structure of the DOS, the low energy excitations in question may proceed from the local occupied peaks in the gap to the lower part of the CB.

The imaginary part of the dielectric function and the oscillator strengths calculated for the $V_NC_B(C_{2v})$ defect are shown in Fig. 10. According to our calculations, the *zz* component of Im(ε) has a negligible magnitude in the energy range of interest, therefore, only the *xx* and *yy* components are shown. We find that the system exhibits a very intense excitation peak in the near-infrared region (1.39 eV), well below the region of interest. However, a more relevant finding about $V_NC_B(C_{2v})$-defected h-BN is the presence of relatively intense excitations in the range $2.12\,\text{eV} < h\nu < 2.33\,\text{eV}$. As mentioned earlier, such peaks might cause the emission observed in Ref. [7]. However, there are two decisive drawbacks of this structure: (i) the peaks of interest are not quite intense—their oscillator strength is five to ten times lower than those found in C_N, for example. These low oscillator strengths are not in agreement with the observed high emission intensity [7]; (ii) as we showed earlier (Sec. IV), the thermodynamic stability of this defect is compromised, and the structure is bound to reconstruct to the geometry of the V_NC_B(corrugated) defect.

E. V_NC_B(corrugated) defect

The structure of the V_NC_B(corrugated) defect is highly corrugated: some N atoms deviate by 0.2 Å above or below the ML plane level, while the C atom is 0.56 Å off plane. This defect reduces the number of valence electrons in the system by 2. Unlike the case of $V_NC_B(C_{2v})$, however, the spin density is zero on all atoms of V_NC_B(corrugated) and thus the magnetization of the supercell is zero. The electronic and optical properties of V_NC_B(corrugated) are strikingly different from those of $V_NC_B(C_{2v})$. Creation of this defect leads to the formation of a narrow and sharp unoccupied peak right next to the bottom of the CB—narrowing the band gap—as well as a sharp and narrow occupied peak slightly below the middle

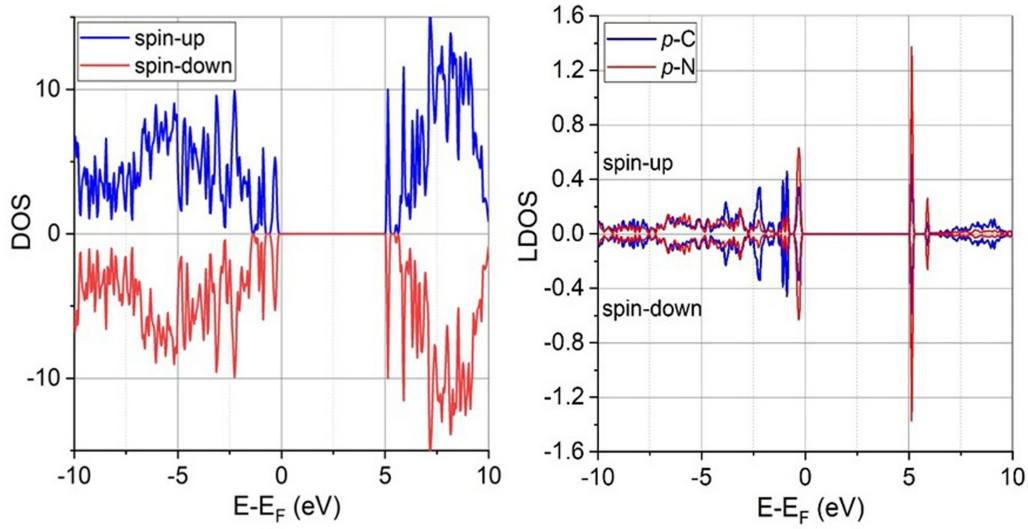

FIG. 13. Electronic structure of the V_NC_B(asymmetric) defected h-BN, calculated within the *GW* approximation. Left panel: total density of IQP states. Right panel: density of the carbon *p* states.

of the band gap (see Fig. 11). Interestingly, the latter peak has a noticeable contribution from the carbon *s* states.

The low energy optical excitations may originate from the local occupied peak in the band gap to the CB. The imaginary part of the dielectric function of the V_NC_B(corrugated) defect is found to have a significant *yy* component within the energy range of interest (see Fig. 12). The *xx* and *zz* components have a negligible magnitude in this area and, thus, are not shown in the figure. There are two peaks of Im(ε) in the region: a moderately high one at $h\nu = 2.7$ eV and a low one around 2.05 eV. The former is characterized by moderately high oscillator strength, but it has an energy much higher than 2.33 eV, which was used in Ref. [7] for excitation. Therefore, this peak cannot induce the observed emission [7]. The other peak has an energy of ∼2.0 eV, which is lower than the observed emission energy 2.12 eV. Assuming some degree of inaccuracy in our calculations, one may conjecture that this absorption peak might induce the observed emission. However, the low oscillation strength of this transition is not in agreement with the observed high emission intensity [7]. We thus conclude that, although the V_NC_B(corrugated) defect is stable, it is unlikely to be the source of the single-photon emission observed in Ref. [7]. Nevertheless, the peak at 2.7 eV indicates that V_NC_B(corrugated) could give rise to single-photon emission still in the visible spectrum but at shorter wavelength than the SPE in question.

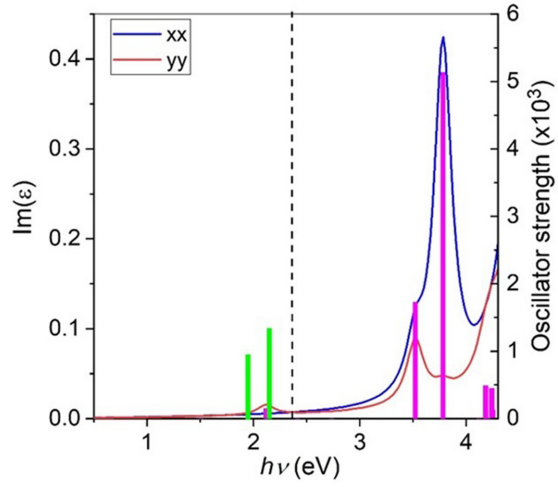

FIG. 14. The imaginary part of the frequency-dependent dielectric function (continuous lines) for *xx* (blue) and *yy* polarization (red), and the oscillator strength of the dipole optical transitions (pink vertical lines) calculated for the V_NC_B(asymmetric) defected h-BN. The green lines mark the energetic positions of the emission detected in Ref. [7]. The dashed black line marks the laser excitation energy 2.33 eV used in Ref. [7].

F. V_NC_B(asymmetric) defect

The V_NC_B(asymmetric) defect causes a significant corrugation of the 2D structure: the C atom and the next-neighboring N atom are found to be off the ML plane by 0.2 and 0.4 Å, respectively, while some other N atoms are shifted in the opposite direction by ∼0.2 Å. The system loses two electrons upon the defect formation, and it is found to be nonmagnetic. This defect also forms local peaks of DOS having the main contribution coming from the *p* states of both C and neighboring N atoms (see Fig. 13). However, in contrast to the other considered defects, these local peaks are located either slightly above the VB or just below the CB. As a result, a wide gap of 5 eV remains between the initial and final states of the possible excitations. Thus, one can expect that excitations in the visible range are not possible. Indeed, as seen from Fig. 14, the imaginary part of the dielectric function has relatively intense peaks only in the UV energy region, $h\nu \sim 3.5$–3.8 eV. These excitations cannot be induced by the laser used in the Ref. [7] experiment, whose energy is only 2.33 eV. Therefore, we conclude that the V_NC_B(asymmetric) defect cannot be the source of the single-photon emission observed in Ref. [7].

Summarizing, our calculations bring us to the conclusion that, among all seven considered defects, only the C_N defect

has an excitation spectrum suitable for inducing the single-photon emission observed in Ref. [7], and it is the most thermodynamically stable.

VI. CONCLUSIONS

The goal of this work is to identify the source of the 2.12-eV single-photon emission in C-doped h-BN reported in Ref. [7]. To this end, we have evaluated the thermodynamic stability of seven C-doping related defects in h-BN, including some that have already been proposed or studied with limited methods: C_B, C_N, C_NN_B, V_BC_N [7,13], $V_NC_B(C_{2v})$ [10], V_NC_B(corrugated), and V_NC_B(asymmetric). We calculated the formation energy for the above defects using a DFT-based method and found E_{form} to be positive for all considered defects, with the lowest values for C_B and C_N, and the highest value for the V_BC_N defect. The phonon spectra calculations showed that all considered defects, except for V_BC_N, are dynamically stable. Namely, the V_BC_N defect has a vibrational mode mostly involving C with an imaginary frequency of 23.94 meV. By perturbing the structure as hinted at by the displacement pattern of the unstable mode of the V_BC_N, we pursued the structural rerelaxation such system would ensue, and found another saddle-point configuration. Application of this perturbation-rerelaxation procedure several times brought the structure to the V_NC_B(corrugated) configuration. We thus conclude that the V_BC_N defect—earlier considered as a possible source of the SPE [7,13]—is unstable and, if formed, would transform to V_NC_B(corrugated). $V_NC_B(C_{2v})$, which is another proposed defect as the source of the SPE [10], is found to be a dynamically stable but very shallow local minimum that reconstructs to V_NC_B(corrugated), and changes its magnetization state if the C atom displaces off plane by ∼0.1Å. The importance to attest the dynamical stability of any proposed structure is stressed by defects V_BC_N and $V_NC_B(C_{2v})$, both of which have been studied earlier as possible SPE but are dynamically and thermodynamically unstable, respectively.

Next, using the *GW* method, we calculated the electronic structure of the six dynamically stable defects within the linear response approximation. The analysis of the calculated IQP DOS shows that the defects lead to the formation of narrow DOS peaks within the band gap with different locations with respect to the VB and the CB, depending on the defect. We find that not only does the number of electrons brought to or removed from the system upon the defect formation determine the magnetic state of the system but also the local geometry. The change in number of electrons also determines whether the local DOS peaks formed within the band gap are occupied or unoccupied.

The intense single-photon emission reported in Ref. [7] had an energy of $h\nu = 2.12$ eV and was excited by a laser with a photon energy of 2.33 eV. Thus, the necessary condition for this emission is the presence of intense peaks in the excitation spectrum with $2.12\,\text{eV} < h\nu < 2.33\,\text{eV}$. To find such excitations in the considered defects, we performed calculations of the frequency-dependent dielectric function and corresponding oscillator strengths using our *GW* results and applying the BSE-based technique. The analysis of our calculations brings us to the conclusion that only the C_N defect has the excitation peaks suitable for the emission observed in Ref. [7]. Finally, although only C_N may explain the single-photon emission observed in Ref. [7], defects C_B and V_NC_B(corrugated) may also be sources of single-photon emission but at different wavelengths in the near-infrared and visible light regions.

It would be interesting to visualize the path of the carbon atom, as it makes the V_BC_N-V_NC_B(corrugated) transformation, to know how and at which temperature $V_NC_B(C_{2v})$ transforms into V_NC_B(corrugated) and, perhaps more importantly, to investigate if any other structure undergoes reconstruction as the temperature increases. *Ab initio* molecular dynamics (MD) simulations would be the ideal tool to answers the questions above. However, the actual path of carbon as it changes its binding site does not affect the conclusion that V_BC_N cannot be the searched-for SPE structure because it is dynamically unstable. Also, a thermal stability investigation of how and at what temperature $V_NC_B(C_{2v})$ reconstructs toward V_NC_B(corrugated) would be desirable if $V_NC_B(C_{2v})$ had any relevant optical properties, but it does not. For the thermal stability of the rest of the structures, one could certainly use *ab initio* MD simulations, however, their dynamical stability and harmonicity for a range of finite displacements in which the total energy increases by up to several tens of meV plus the large binding energy of C indicate that all other structures will be stable at least at room temperature (corresponding to 25 meV).

ACKNOWLEDGMENT

The authors acknowledge the University of Central Florida Advanced Research Computing Center for providing computational resources and support that have contributed to results reported herein [25].

[1] G. Zhang, Y. Cheng, J.-P. Chou, and Adam Gali, Material platforms for defect qubits and single-photon emitters, Appl. Phys. Rev. **7**, 031308 (2020).

[2] S. Ditalia Tchernij, T. Lühmann, T. Herzig, J. Küpper, A. Damin, S. Santonocito, M. Signorile, P. Traina, E. Moreva, F. Celegato *et al.*, Single-photon emitters in lead-implanted single-crystal diamond, ACS Photonics **5**, 4864 (2018).

[3] D. M. Lukin, C. Dory, M. A. Guidry, K. Y. Yang, S. D. Mishra, R. Trivedi, M. Radulaski, S. Sun, D. Vercruysse, G. H. Ahn, and J. Vučković, 4H-silicon-carbide-on-insulator for integrated quantum and nonlinear photonics, Nat. Photonics **14**, 330 (2020).

[4] T. T. Tran, K. Bray, M. J. Ford, M. Toth, and I. Aharonovich, Quantum emission from hexagonal boron nitride monolayers, Nat. Nanotechnol. **11**, 37 (2016).

[5] A. L. Exarhos, D. A. Hopper, R. R. Grote, A. Alkauskas, and L. C. Bassett, Optical signatures of quantum emitters in suspended hexagonal boron nitride, ACS Nano **11**, 3328 (2017).

[6] J. D. Caldwell, I. Aharonovich, G. Cassabois, J. H. Edgar, B. Gil, and D. N. Basov, Photonics with hexagonal boron nitride, Nat. Rev. Mater. **4**, 552 (2019).

[7] N. Mendelson, D. Chugh, J. R. Reimers, T. S. Cheng, A. Gottscholl, H. Long, C. J. Mellor, A. Zettl, V. Dyakonov, P. H. Beton *et al.*, Identifying carbon as the source of visible single-photon emission from hexagonal boron nitride, Nat. Mater. **20**, 321 (2021).

[8] K. Watanabe, T. Taniguchi, and H. Kanda, Direct-bandgap properties and evidence for ultraviolet lasing of hexagonal boron nitride single crystal, Nat. Mater. **3**, 404 (2004).

[9] G. Cassabois, P. Valvin, and B. Gil, Hexagonal boron nitride is an indirect bandgap semiconductor, Nat. Photonics **10**, 262 (2015).

[10] A. Sajid and K. S. Thygesen, V_NC_B defect as source of single photon emission from hexagonal boron nitride, 2D Mater. **7**, 031007 (2020).

[11] A. Sajid, M. J. Ford, and J. R. Reimers, Single-photon emitters in hexagonal boron nitride: A review of progress, Rep. Prog. Phys. **83**, 044501 (2020).

[12] T. J. Smart, K. Li, J. Xu, and Y. Ping, Intersystem crossing and exciton–defect coupling of spin defects in hexagonal boron nitride, NPJ Comput. Mater. **7**, 59 (2021).

[13] Y. Chen and S. Y. Quek, Photophysical characteristics of boron vacancy-derived defect centers in hexagonal boron nitride, J. Phys. Chem. C **125**, 21791 (2021).

[14] L. Hedin, New method for calculating the one-particle green's function with application to the electron-gas problem, Phys. Rev. **139**, A796 (1965).

[15] G. Onida, L. Reining, and A. Rubio, Electronic excitations: Density-functional versus many-body Green's-function approaches, Rev. Mod. Phys. **74**, 601 (2002).

[16] G. Kresse and G. J. Furthmüller, Efficient iterative schemes for ab initio total-energy calculations using a plane-wave basis set, Comput. Mater. Sci. **6**, 15 (1996).

[17] G. Kresse and J. Joubert, From ultrasoft pseudopotentials to the projector augmented-wave method, Phys. Rev. B **59**, 1758 (1999).

[18] J. P. Perdew, S. Burke, and M. Ernzerhof, Generalized Gradient Approximation Made Simple, Phys. Rev. Lett. **77**, 3865 (1996).

[19] M. Shishkin and G. Kresse, Implementation and performance of the frequency-dependent GW method within the PAW framework, Phys. Rev. B **74**, 035101 (2006).

[20] S. S. Mitra, Combination of the lattice modes with the internal modes in a crystal, J. Chem. Phys. **39**, 3031 (1963).

[21] M. Alcántara Ortigoza, R. Heid, K. P. Bohnen, and T. S. Rahman, Anomalously soft and stiff modes of transition-metal nanoparticles, J. Phys. Chem. C **118**, 10335 (2014).

[22] M. Alcántara Ortigoza, R. Heid, K. P. Bohnen, and T. S. Rahman, Nature of the binding of a c(2 × 2)-CO Overlayer on Ag(001) and surface mediated intermolecular coupling, J. Phys. Chem. A **115**, 7291 (2011).

[23] G. Noh, D. Choi, J.-H. Kim, D.-G. Im, Y.-H. Kim, H. Seo, and J. Lee, Stark tuning of single-photon emitters in hexagonal boron nitride, Nano Lett. **18**, 4710 (2018).

[24] A. Sajid, J. R. Reimers, and M. J. Ford, Defect states in hexagonal boron nitride: Assignments of observed properties and prediction of properties relevant to quantum computation, Phys. Rev. B **97**, 064101 (2018).

[25] https://arcc.ist.ucf.edu.